MATERIALS SCIENCE

Flexible ferroelectric element based on van der Waals heteroepitaxy

Jie Jiang,[1]* Yugandhar Bitla,[2]* Chun-Wei Huang,[2] Thi Hien Do,[3] Heng-Jui Liu,[4] Ying-Hui Hsieh,[2] Chun-Hao Ma,[5] Chi-Yuan Jang,[6] Yu-Hong Lai,[2] Po-Wen Chiu,[5] Wen-Wei Wu,[2] Yi-Chun Chen,[6] Yi-Chun Zhou,[1†] Ying-Hao Chu[2,3,7†]

2017 © The Authors, some rights reserved; exclusive licensee American Association for the Advancement of Science. Distributed under a Creative Commons Attribution NonCommercial License 4.0 (CC BY-NC).

We present a promising technology for nonvolatile flexible electronic devices: A direct fabrication of epitaxial lead zirconium titanate (PZT) on flexible mica substrate via van der Waals epitaxy. These single-crystalline flexible ferroelectric PZT films not only retain their performance, reliability, and thermal stability comparable to those on rigid counterparts in tests of nonvolatile memory elements but also exhibit remarkable mechanical properties with robust operation in bent states (bending radii down to 2.5 mm) and cycling tests (1000 times). This study marks the technological advancement toward realizing much-awaited flexible yet single-crystalline nonvolatile electronic devices for the design and development of flexible, lightweight, and next- generation smart devices with potential applications in electronics, robotics, automotive, health care, industrial, and military systems.

INTRODUCTION

Ferroelectric materials (*1*, *2*) with switchable spontaneous polarization, superior pyroelectricity, and piezoelectricity are exploited in the applications of nonvolatile memory (NVM) (*3*–*5*), logic (*6*), memristor (*7*), sensors, and actuators (*8*). Currently, the surge to develop next-generation smart electronics in light of "internet of things" demands the integration of various functionalities with conventional electronic systems. Flexible electronics (*9*, *10*) is one such attribute that has attracted long-standing attention in today's energy-conscious world owing to their advantages of excellent portability, bendability, being lightweight and human-friendly interfaces. Consequently, the realization of flexible electronics in display, sensor, biomedical, and industrial applications has necessitated the design and development of flexible logic and memory elements for information storage, data processing, and communication. Continuous efforts are being put forward to realize high-speed, high-storage density, low-power, low-cost, light-weight, and yet flexible electronic components. Perovskite lead zirconium titanate [$Pb(Zr,Ti)O_3$; PZT] (*11*) having large polarization, fast polarization switching, high Curie temperature, low coercive field, and a high piezoelectric coefficient, is probably the most explored system for these applications. The flexible version of polycrystalline PZT–based NVM has been demonstrated on Si (*12*, *13*), Pt foil (*14*), Cu foil (*15*), and Ni superalloy ribbons (*16*) or built on Si and then transferred on to flexible polymer substrates (*17*, *18*). It has long been postulated that single-crystalline functional oxides could resolve the critical issue of memory retention time in current technologies. However, the integration of superior device performance of the single-crystalline PZT with the current conventional flexible substrates is severely impeded by its lack of high-temperature growth, which causes leakage and electrical shorting with degraded device performance. As a result, all the polycrystalline PZT–based ferroelectric memories underperform because of the lack of an appropriate flexible substrate. Nevertheless, much of the current research is focused on the low-cost and low-temperature polymer ferroelectrics (*19*–*24*), which often exhibit very limited thermal and operational stabilities besides their inferior field mobilities. These drawbacks can be potentially solved by the fabrication of flexible organic ferroelectric crystals. However, the performance in the device level is not tested yet (*25*). Recently, the integration of the single-crystalline PZT with Si has been demonstrated (*26*). However, the transfer of epitaxial PZT at room temperature involves a tedious multistep process. Therefore, to obtain high crystalline quality of ferroelectric materials with superior properties, the proper choice of flexible substrate and electrode must be made for device applications.

Here, a model ferroelectric PZT system is demonstrated to build up a ferroelectric element based on oxide heteroepitaxy for flexible electronics. We present the realization of epitaxial PZT ($PbZr_{0.2}Ti_{0.8}O_3$) on mica for flexible NVM applications (Fig. 1). The key advantages of adopting a muscovite mica substrate include its atomically smooth surface, high thermal stability (T_M ~ 1000°C), chemical inertness, high transparency, mechanical flexibility, and compatibility with present fabrication methods. The monoclinic muscovite mica, $KAl_2(AlSi_3O_{10})(OH)_2$, has a two-dimensional (2D) structure with an AlO_6 octahedral layer sandwiched by two $(Si,Al)O_4$ tetrahedral layers, which are stacked further by a layer of potassium cations. This 2D layered material can be mechanically exfoliated like graphene down to few tens of micrometers. The heteroepitaxy involving 2D materials is categorized as van der Waals (vdW) epitaxy (*27*). Initially, vdW epitaxy strictly implied the growth of 2D material on another 2D material substrate, but later, it got extended to the heteroepitaxial growth of 2D materials onto 3D substrates or vice versa. The 2D/3D or 3D/2D materials result from the quasi-vdW epitaxy process, which is an intermediate to conventional and vdW epitaxies (*28*). Direct growth of functional oxides (*29*–*32*) on muscovite via the vdW epitaxy has been demonstrated recently in view of flexible device applications. This approach does not impose requirements of overcoming the issue of lattice mismatch between the film and substrate that results in a significant reduction of defect density. Moreover, a weak vdW interaction between the film and substrate can further reduce the substrate clamping effect, favoring better device performance. Figure 1 (A and B) shows the design and an actual flexible

[1]Key Laboratory of Low Dimensional Materials and Application Technology of Ministry of Education, Xiangtan University, Hunan 411105, China. [2]Department of Materials Science and Engineering, National Chiao Tung University, Hsinchu 30010, Taiwan. [3]Institute of Physics, Academia Sinica, Taipei 11529, Taiwan. [4]Department of Materials Science and Engineering, National Chung Hsing University, Taichung 40227, Taiwan. [5]Institute of Electronics Engineering, National Tsing Hua University, Hsinchu 30013, Taiwan. [6]Department of Physics, National Cheng Kung University, Tainan, Taiwan. [7]Material and Chemical Research Laboratories, Industrial Technology Research Institute, Hsinchu 31040, Taiwan.
*These authors contributed equally to this work.
†Corresponding author. Email: zhouyc@xtu.edu.cn (Y.-C.Z.); yhc@nctu.edu.tw (Y.-H.C.)

Downloaded from http://advances.sciencemag.org/ on June 11, 2017

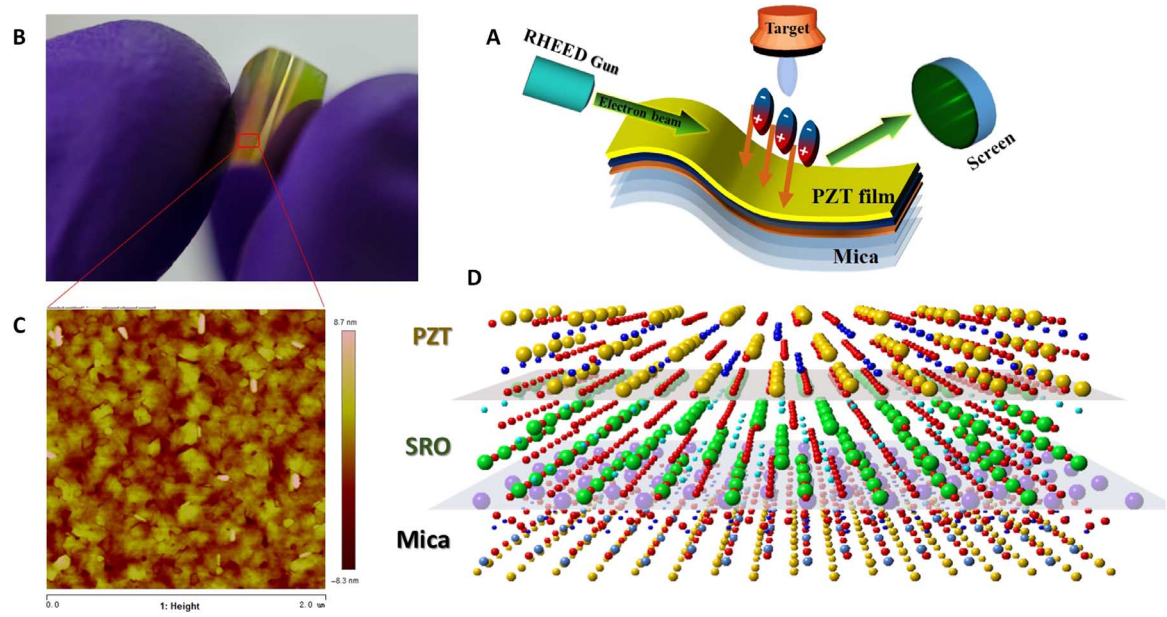

Fig. 1. Flexible memory design. Growth scheme (**A**) and photograph (**B**) of a flexible NVM element on mica. RHEED, reflection high-energy electron diffraction. (**C**) Atomic force micrograph. (**D**) Schematic illustration of PZT/mica heterostructure via vdW heteroepitaxy.

NVM element based on PZT. Figure 1C shows the surface morphology of the flexible heterostructure by an atomic force microscopy over a measurement area of 2 × 2 μm^2. The film exhibits an average surface roughness (R_a) of 0.62 nm and root mean square roughness (R_{rms}) of 0.81 nm, indicating a very smooth surface. Figure 1D shows the schematic of the heterostructure at atomic level wherein 3D functional perovskites, including metallic $SrRuO_3$ (SRO) and ferroelectric PZT epitaxial layers, grow on top of mica sheets. This work marks a critical milestone in the advancement of flexible ferroelectric elements via vdW oxide heteroepitaxy that not only retain the superior properties of epitaxial films but also exhibit mechanical flexibility, durability, and thermal stability.

RESULTS

The phase identification and crystal structure of the heterostructures were examined by a Taiwan synchrotron x-ray diffraction (XRD) facility. In the heterostructure, a very thin $CoFe_2O_4$ (CFO) layer was grown as the seeding layer for the growth of high-quality perovskites, including a SRO layer as the bottom electrode for electrical characterizations. The choice of perovskite SRO electrode was deliberately made because it not only presents excellent lattice, structural, and chemical compatibility with PZT but also acts as a sink for oxygen vacancies and thus prevents serious fatigue behavior of polarization often encountered in PZT capacitors with metal electrodes (*33*). Figure 2A shows a typical out-of-plane 2θ-θ scan of the heterostructure. The observation of only PZT(*lll*) and SRO(*lll*) diffraction peaks with muscovite (00*l*) suggests the epitaxial nature of thin films without other secondary phases. The estimated interplanar spacing for PZT (d_{111} = 2.365 Å) and SRO (d_{111} = 2.301 Å) suggests tensile strains of 1.9 and 0.6%, respectively. Furthermore, the Φ scans of PZT{002}, SRO{002}, CFO{004}, and muscovite{202} reflections were used to analyze the in-plane structural relationships, as shown in Fig. 2B. The observation of three muscovite {202} peaks at 120° intervals indicates different stacking sequences between sheet units along the *c* axis (*34*), whereas SRO{002} and PZT{002} exhibit six peaks that indicate the growth of epitaxial SRO and PZT films with a multidomain feature on mica substrate. On the basis of the XRD results, the epitaxial relationships can be determined as $(111)_{SRO}//(111)_{PZT}//(001)_{mica}$ and $[1\text{-}10]_{SRO}//[1\text{-}10]_{PZT}//[010]_{mica}$ for the heterostructure. To unveil the detailed structural information, we recorded the reciprocal space mapping of PZT(002), SRO(002), and CFO(004) reflections using the basis of mica reciprocal lattice (Fig. 2C), which also confirms the same epitaxial relationships obtained above. The estimated interplanar spacing of 2.360 Å for PZT in an out-of-plane (1.222 Å in in-plane) direction suggests tensile strain of 1.8% (compressive strain of 1.4%) in accordance with the XRD result. These results are further corroborated by the in situ RHEED results presented in fig. S1. To characterize the detailed microstructure on the heteroepitaxy of PZT/mica, we examined the film-substrate interface using transmission electron microscopy. Figure 2D shows cross-sectional TEM images taken along the zone axis of $[010]_{mica}$, revealing PZT/SRO and SRO/CFO/mica interfaces together with the selected area diffraction patterns of PZT, SRO, and mica. The reciprocal lattices are also clearly indexed, and the consistency of epitaxial relationships with the XRD results is further confirmed. The sharp interfaces without observable interdiffusion of species across the interfaces indicate high quality of the heterostructure.

Building a quantitative and comprehensive knowledge of the heterostructure characteristics is crucial for ongoing research and development in the necessary manufacturing processes for designing numerous flexible smart devices. To characterize the ferroelectricity of the heterostructure, piezoresponse force microscopy (PFM) (*35*) is an ideal tool for both probing and switching the local ferroelectric polarization at nanoscale. The box-in-box switched patterns were written on the PZT layer, with the application of electric field via a conducting tip. A tip bias of −8 V was applied to pole the 3 µm × 3 µm square region, followed by another poling with a tip bias of +8 V in the central area of 1 µm × 1 µm. The surface topography and the corresponding out-of-plane and in-plane polarization signals are shown in Fig. 3 (A and C). In Fig. 3B, a PFM phase image shows clear bright and dark contrast regions corresponding to upward and downward polarizations, respectively. After the poling, the area

Downloaded from http://advances.sciencemag.org/ on June 11, 2017

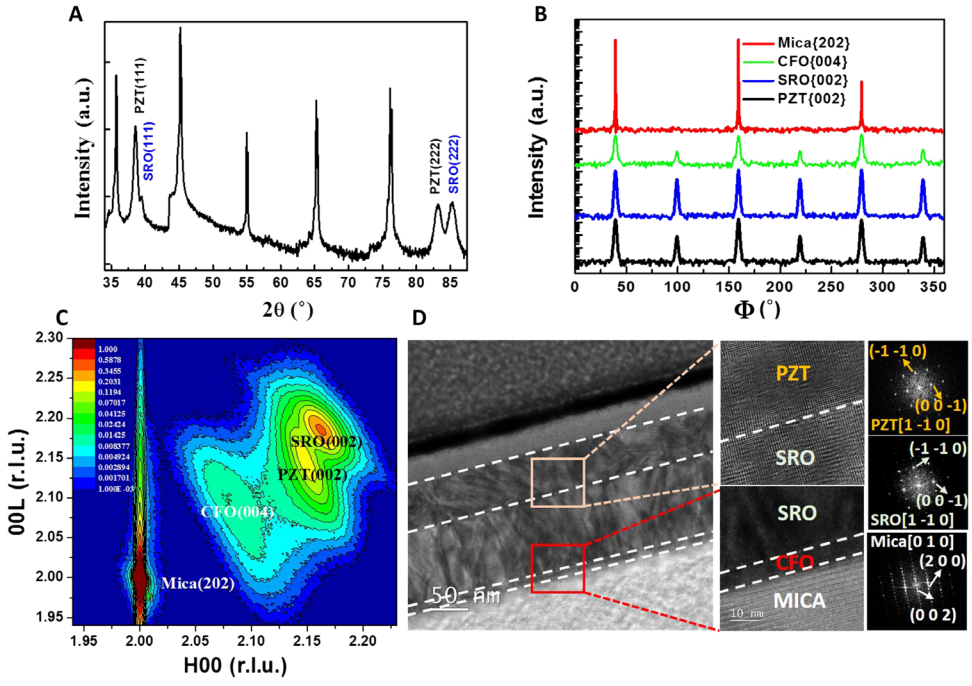

Fig. 2. Structural information. (**A**) Typical 2θ-θ scan of the heterostructure. (**B**) Φ scans at PZT{002}, SRO{002}, CFO{004}, and mica{202} diffraction peaks. a.u., arbitrary units. (**C**) The reciprocal space mapping of the heterostructure. r.l.u., relative light units. (**D**) The cross-sectional TEM image depicting the PZT/SRO and SRO/CFO/mica interfaces along with the selected area diffraction patterns of PZT, SRO, and mica.

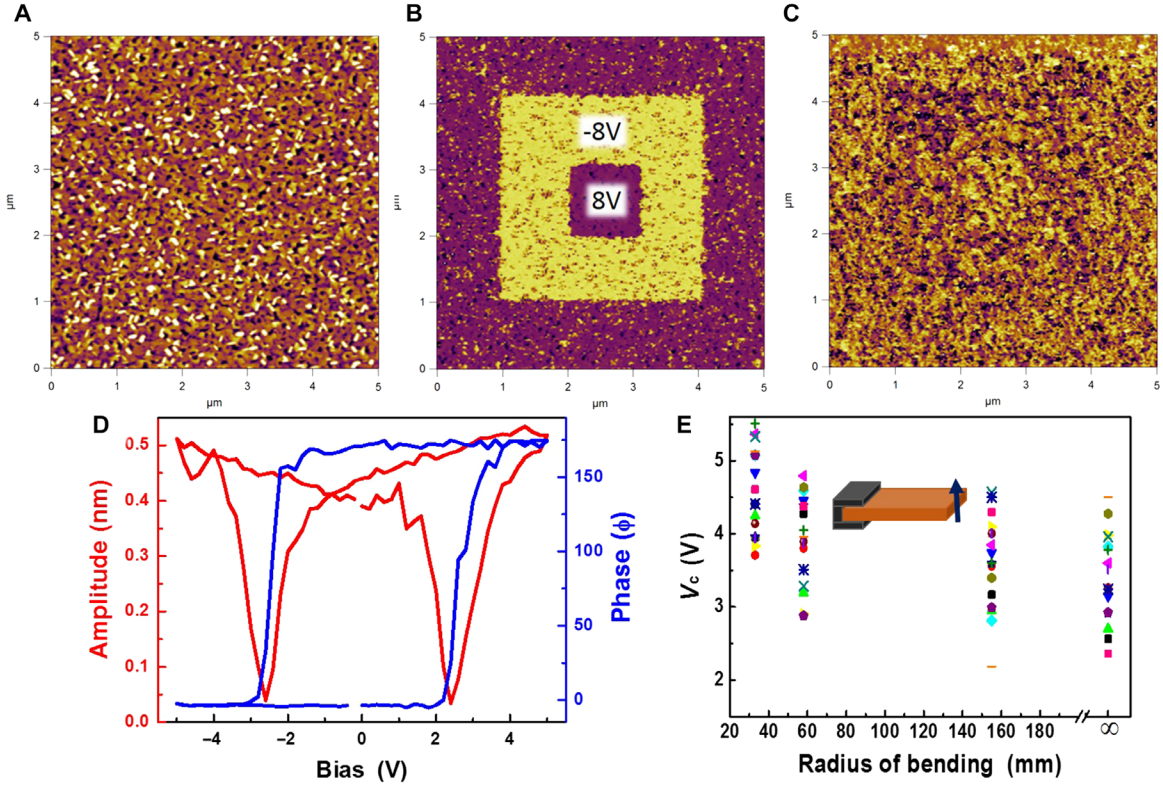

Fig. 3. Piezoresponse force microscopy. The surface topography (**A**) with out-of-plane (**B**) and in-plane phase (**C**) images. (**D**) Representative local PFM amplitude and phase hysteresis loops. (**E**) The local coercive voltage variation as a function of bending radius.

Downloaded from http://advances.sciencemag.org/ on June 11, 2017

between 3 μm × 3 μm and 1 μm × 1 μm shows bright contrast and dark contrast in the 1 μm × 1 μm area. This result suggests that polarization of PZT layer is switchable, confirming the ferroelectric nature of the heterostructure. Furthermore, the in-plane phase image, wherein the contrast is random before and after the poling, asserts the multidomain state of the PZT film. Typically, in this composition of PZT, the direction of ferroelectric polarization points along [001]. Thus, the multidomain feature is attributed to the (111) orientation of the heterostructure. Moreover, local PFM loops were measured across the film in a 5 × 4 grid, resulting in 20 data points (fig. S2A). Figure 3D shows representative local PFM amplitude and phase hysteresis loops. The square loop demonstrating a 180° change in PFM phase and a clear butterfly loop in PFM amplitude confirms a good ferroelectric switching nature of the heterostructure. The local coercive voltages are ~2.4 and −2.6 V, indicated by the minima of the amplitude loop, suggesting a symmetric loop without a strong ferroelectric imprint. The PZT/SRO/mica was tested further to explore the mechanical strain effect on its local ferroelectricity (Fig. 3E), corresponding to different locations marked in fig. S2A. The sample was compressively bent, as depicted by the schematic in the inset (see also fig. S2, B and C, for description). The local coercive fields of unbent state increased slowly under bending, suggesting a slight change of local ferroelectricity with the strain.

The advances in the emerging flexible electronic devices motivate researchers to explore additional requirements of NMV elemental stability in harsh environments (*13*). Well-saturated and symmetric polarization-electric field (*P-E*) hysteresis loops and the capacitance-electric field (*C-E*) or the "butterfly" curves of the heterostructure measured at 1 MHz and temperatures ranging from 25° to 175°C for a virgin device are shown in Fig. 4 (A and B, respectively). The typical square hysteresis loop with a sharp change in polarization shows effective switching of the dipoles. The ferroelectric capacitor exhibits a saturation polarization (P_{sat}) of ~75 μC/cm^2, a remnant polarization (P_r) of ~60 μC/cm^2, and a coercive field (E_c) of ~100 kV/cm at 25°C, and the temperature evolution is shown in Fig. 4C. The estimated dielectric constant variation along with temperature-dependent capacitance is shown in fig. S3. The polarization switching kinetics at different voltage levels shown in Fig. 4D were evaluated using a sequence of fast voltage pulses for the standard positive-up and negative-down (PUND) method (*5*). As shown in the inset of Fig. 4D, the device is initially preset to a negative polarized state (P_1) at −4 V, followed by voltage pulses to measure switching polarization (P_2) from negative to positive and switched polarization at 4 V (P_3) in the positive region, respectively. The pulsed switched polarization, $\Delta P = P_3 - P_2$, as a function of pulse width (Fig. 4D) shows that the switching speed increases as the voltage increases. The ΔP (105 μC/cm^2) is approximately 1.8 times that of P_r. Thus, the presence of intrinsic ferroelectricity in PZT/mica system is confirmed. For these ferroelectric capacitors to be used in NVM applications, ferroelectric reliability issues, such as imprint, retention, and fatigue, have to be addressed for their long lifetime operation. These NVM cells exhibit excellent retention (Fig. 4E) even after 10^5 s at room temperature as well as at high temperatures, meeting the most important criteria of memory application. The retention time of 10^5 s at 100°C corresponds to retention time of 10 years at 69°C. This is the best value reported so far among the flexible NVMs (*12*–*24*, *26*) because of their superior crystalline quality. The polarization fatigue, which is the reduction in the amount of remnant polarization with repeated switching cycles, of a PZT/mica capacitor is displayed in Fig. 4F. It is interesting to see a noticeable improvement in fatigue behavior at high temperature. The device maintained switching ability at room temperature up to

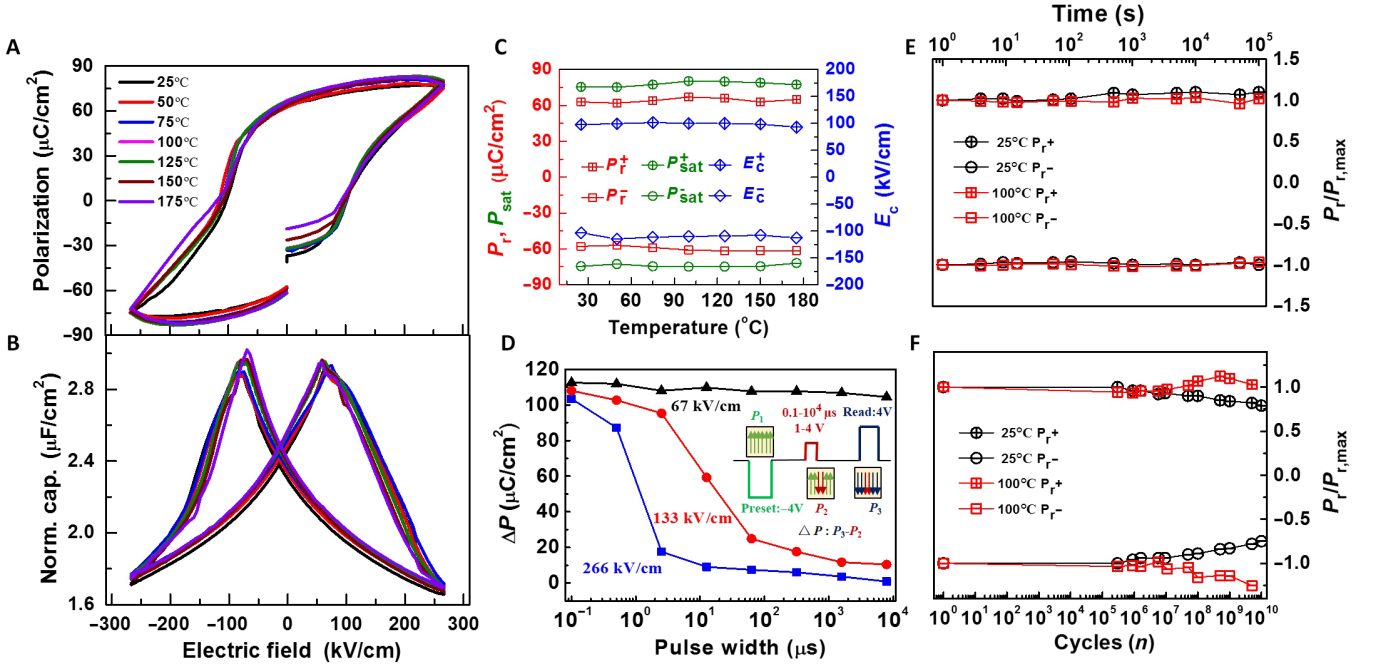

Fig. 4. Ferroelectric properties. *P-E* (**A**) and *C-E* (**B**) hysteresis loops at various temperatures. (**C**) Remnant, saturation polarizations, and coercive field as functions of temperature. (**D**) PUND switching polarization as a function of pulse width at different voltages. The inset shows the measurement sequence. Retention (**E**) and fatigue (**F**) measurements at two typical temperatures.

Downloaded from http://advances.sciencemag.org/ on June 11, 2017

10^7 cycles, whereas at high temperature, fatigue resistance was maintained until 10^{10} cycles. This behavior can be attributed to PZT quality and underlying mica's high-temperature stability. It is clear from the aforementioned results that PZT/mica heterostructure can play a potential key role in high-temperature electronic applications.

To extend the practical applications of this flexible ferroelectric system, a series of cyclability tests were carried out. The macroscopic ferroelectric performance of the heterostructure against mechanical flexing was evaluated under both tensile and compressive bendings (*31*). Figure 5 (A and B) shows the *P-E* and *C-E* hysteresis loops of the PZT capacitors under various compressive and tensile bending radii (*r*), whereas Fig. 5C shows the change in P_{sat}, P_r, and E_c values as a function of bending radius and corresponding strains (see the Supplementary Materials for more details). For the bending radius down to 2.5 mm, an observation of constant P_{sat}, P_r, and E_c values within experimental errors suggests that the PZT thin-film capacitor shows stable electrical properties even under mechanical constraints. The estimated dielectric constant variation along with mechanical flexing–dependent capacitance and the dielectric constant are shown in fig. S4. Moreover, the *P-E* hysteresis loops under tensile and compressive bending of 5 mm before and after 10 to 1000 bending cycles obtained from the capacitor structure exhibited no noticeable change (see fig. S5). Figure 5D depicts the ΔP as a function of pulse width at 4 V under compressive as well as tensile flexing (complete data at different voltage pulses are shown in fig. S6). The inset shows the polarization switching speed as a function of bending radius and strain at two different switch voltage pulses. The switching speed increases with switching pulse and is unaltered irrespective of the nature of mechanical bending. Therefore, it can be concluded that the polarization switching kinetics of PZT/mica are robust against mechanical flexing. Figure 5E displays stable polarization retention of capacitors irrespective of physical bending states. It is noteworthy that these capacitors continue to exhibit this robust retention capability even after being mechanically flexed for 1000 cycles. Furthermore, Fig. 5F shows the evolution of the normalized polarization as a function of the number of switching cycles. The fatigue behavior is stable in bent states and remains identical before and after 1000 tensile bending cycles as well as compressive bending cycles. Almost no polarization fatigue is seen until 10^7 switching cycles; however, it reduces to 33% of its initial value after 10^{10} cycles for the unbent and tensile flexing samples, whereas compressive flexing improves the behavior. Therefore, it is evident from Fig. 5 that the fabricated PZT memory elements exhibit stable and superior performance against mechanical bending highly desirable for flexible device applications. These values of mechanical tolerance are the best among all the NVM elements. The physical strain imposed on the heterostructure under different mechanical flexing is examined by Raman spectroscopy, as shown in fig. S7. The maximum strain generated depends on thin film–substrate interface, mechanical property of the mica and its thickness, and the radius of bending. The results of Raman spectroscopy show a negligible imposed strain under the bending. This result could be attributed to the slide of mica sheets and the weak vdW interaction between the mica substrate and ferroelectric capacitor as well as the multidomain feature of PZT film.

DISCUSSION

A comparison is made between the flexible heteroepitaxial system in this study and the currently reported ferroelectric-based flexible thin films in Table 1. It is clear from the table that the PZT/mica system has the best performance metrics among all the flexible NVM elements because of its superior crystalline quality. The epitaxial and flexible PZT/mica heterostructures reported in this work find applications not only as memory elements for information technology but also as nanogenerators (*36*) and energy harvesters for biomedical application (*37*). Because of the biocompatibility of mica, these heterostructures with proper PZT layer packaging can be attached to conformal geometry of various organs and deliver the energy-harvesting functionality. This is possible due to the fact that these heterostructures can deliver the best piezoelectric coefficients via vdW epitaxy that results in very weak interaction between PZT and mica, minimizing substrate clamping

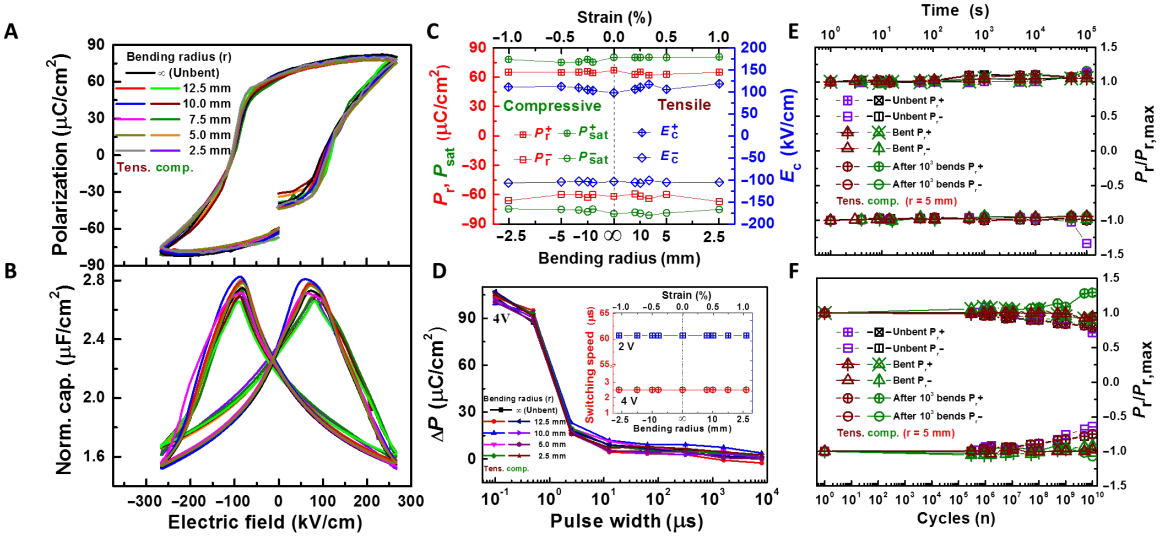

Fig. 5. Flexibility and durability. *P-E* (**A**) and *C-E* (**B**) hysteresis loops under various tensile and compressive bending radii. (**C**) P_{sat}, P_r, and E_c variation as a function of bending radius. (**D**) ΔP as a function of pulse width at 4 V under mechanical flexing. Polarization switching speed variation is shown in the inset. Retention (**E**) and fatigue (**F**) for the samples in unbent and compressively and tensilely bent for 1000 cycle conditions.

Downloaded from http://advances.sciencemag.org/ on June 11, 2017

Table 1. Flexible memory elements. Summary of the flexible NVM elements. PZT*x*, $PbZr_xTi_{1-x}O_3$; P(VDF-TrFE), poly[(vinylidenefluoride)-*co*-trifluoroethylene]; BTO, barium titanate; PET, polyethylene terephthalate; PI, polyimide; PEN, polyethylene naphthalate.

Ferroelectric material	PZT20*	PZT20*	PZT52†	PZT52	PZT53	PZT30	PZT52	PZT	BTO	P(VDF-TrFE)			
Flexible substrate	Mica	Si	Ni superalloy ribbons	Si	Pt foil	PI	Cu foil	Plastic	PET	Al foil	Organic	PEN	PI
Transfer required	No	Yes	No	No	Yes	No	No	Yes	No	Yes	No	No	No
P_r ($\mu C/cm^2$)	60	75	40	18	25.5	15	20	~20	—	11	7.4	8.52	—
E_c (kV/cm)	100	400	91	60	54.9	~500	~25	1.1 V	—	830	500	650	—
Capacitance (F/cm^2)	2.85	~1.6	—	4	—	—	—	2.7	—	—	0.062	—	—
Dielectric constant	460 @ 1 MHz	—	—	541 @ 1 kHz	—	80 @ 1 kHz	~1150	—	250 @ 0.1 MHz	—	—	—	—
Switching time (ns)	2000	—	—	500	—	165	—	—	—	—	—	—	—
Fatigue (cycles)	$>10^{10}$ (unbent) $>10^{10}$ (bent)	—	—	$>10^9$ (unbent) $>10^{10}$ (bent)	10^7	15% loss @ 10^7	10^{10}	—	—	—	—	—	10^2
Retention (years)	>10 (unbent) >10 (bent)	—	—	>10	—	20% loss @ 10^5 s	—	—	—	—	—	—	>7000 s
Cell size (mm^2)	0.00785–0.0314	0.0484	0.00785–0.0471	0.01–0.0625	0.008	0.03	—	0.01	16	0.025	0.03–0.25	—	—
Minimum bending radius (mm)	2.5	—	—	5	—	—	—	8	—	6	—	7	0.5
Bending cycles @ radius	>1000 @ 5 mm	—	—	1000 @ 5 mm	—	—	—	—	—	500 @ 11 mm	—	—	>1000 @ 4 mm
Reference	This work	(*26*)	(*16*)	(*12*, *13*)	(*14*)	(*18*)	(*15*)	(*17*)	(*39*)	(*19*)	(*20*)	(*21*)	(*22*)

*Single-crystalline. †Highly oriented.

unlike other reported PZT thin films so far. Recently, a flexible piezoelectric energy harvester based on PZT/PI was used to collect mechanical energy of organ's contraction and relaxation of the heart, lung, and diaphragm of different animals (*38*). This research is continuously motivated by the quest to eliminate, or less frequently replace, batteries; it allows researchers to explore new avenues toward realizing more efficient human organ implants. The successful integration of biocompatible microelectromechanical systems is anticipated to trigger a whole new range of possibilities in wearable and implantable electronics. In conclusion, high-quality epitaxial yet flexible ferroelectric PZT for NVM applications is successfully demonstrated. Furthermore, these heterostructures retain the superior performance of their epitaxial counterpart yet display good performance at elevated temperatures.

MATERIALS AND METHODS

Materials

Sample preparation

The epitaxial $PbZr_{0.2}Ti_{0.8}O_3$ (PZT) thin film was deposited on freshly cleaved muscovite mica via pulsed laser deposition using a PZT target. The deposition chamber was initially evacuated to a base pressure of 10^{-7} Torr. The deposition process was carried out at a substrate temperature of 630°C in an oxygen pressure of 100 mTorr, with a KrF excimer laser (λ = 248 nm; Coherent) operated at a laser repetition rate of 10 Hz and a laser energy of 250 mJ. However, before SRO and PZT deposition, a CFO buffer layer (<10 nm) was deposited at a substrate temperature of 590°C in an oxygen pressure of 50 mTorr.

METHODS

Structural characterization

The room temperature 2θ-θ scan along normal direction, Φ scans, RHEED, and reciprocal space mapping was used to obtain structural information. The surface morphology was investigated by an atomic force microscope, whereas the film-substrate interface microstructure was studied by cross-sectional TEM performed at room temperature on FEI Tecnai at 200 kV. The samples were cut by focused ion beam to reveal the interface information. Micro-Raman spectra were measured by a backscattering confocal microscope (MFO, Horiba Jobin Yvon) equipped with an excited 532-nm solid-state laser and a spectrometer (iHR550, Horiba Jobin Yvon). The laser was focused on the sample using a 100× objective.

PFM measurement

PFM was performed via the Asylum Research Cypher under ambient conditions with the homemade bending stage to investigate the evolution of ferroelectricity when sample was under bending. The phase-voltage hysteresis loops were measured by Olympus PtIr-coated Si

Downloaded from http://advances.sciencemag.org/ on June 11, 2017

probes (spring constant, k ~ 2 N/m; tip radius, ~25 nm) superimposed with a 1-Hz triangular square-stepping wave with a bias window up to 8 V, and each loop was averaged over five consecutive cycles.

Bending tests

Predesigned Teflon molds of fixed bending radii were used to induce the reported compressive and tensile bending strains. PZT/mica with bottom electrodes was attached to these molds using double-sided tape. Care was taken to avoid the slipping/gliding of mica during the measurement. For bending cycles measurement, computer-aided homebuilt bending setup combined with optical microscope was used. The PZT/mica was bent from one end with the aid of a motor, whereas the other end was fixed, and the vertical distance was measured using the microscope. The setup allows the length of the sample to be bent by providing the displacement as small as 1 μm on the bending stage. One can set arbitrary bending radii as well as perform bending cycles.

P-E measurement

The ferroelectric properties were analyzed by ferroelectric test systems (Radiant Technologies Precisions workstations RT66A). The polarization-electric field (*P-E*) hysteresis loops were measured by two tips with a frequency of 2 kHz at 4 V, and different radii were checked by using the bending stage. The temperature change measurement system was used to estimate *P-E* variation along with temperature ranging from 25° to 175°C.

C-E measurement

The dielectric properties of the films were measured using a semiconductor device analyzer (Agilent B1500A). The capacitance-electric field (*C-E*) curves were measured by two tips with a frequency of 1 MHz at 4 V, and different radii were checked by using the bending stage. The temperature change measurement system was used to estimate dielectric properties variation along with temperature ranging from 25° to 175°C.

SUPPLEMENTARY MATERIALS

Supplementary material for this article is available at http://advances.sciencemag.org/cgi/content/full/3/6/e1700121/DC1

Supplementary Text

fig. S1. RHEED pattern.

fig. S2. Piezoresponse force microscopy.

fig. S3. Dielectric constant and capacitance at different temperatures.

fig. S4. Dielectric constant and capacitance under bending.

fig. S5. *P-E* hysteresis loops under tensile and compressive bending of 5 mm before and after 10 to 1000 bending cycles.

fig. S6. ΔP as a function of pulse width at various voltage pulses under compressive and tensile strains.

fig. S7. Raman spectra under bending.

References (*40*–*43*)

REFERENCES AND NOTES

1. R. Ramesh, Ed., *Thin Film Ferroelectric Materials and Devices* (Springer, 1997).
2. Y. Xu, *Ferroelectric Materials and Their Applications* (North-Holland, 1991).
3. J. F. Scott, *Ferroelectric Memories* (Springer, 2000).
4. S.-T. Han, Y. Zhou, V. A. L. Roy, Towards the development of flexible non-volatile memories. *Adv. Mater.* **25**, 5425–5449 (2013).
5. M. T. Ghoneim, M. M. Hussain, Review on physically flexible nonvolatile memory for internet of everything electronics. *Electronics* **4**, 424–479 (2015).
6. J. Hoffman, X. Pan, J. W. Reiner, F. J. Walker, J. P. Han, C. H. Ahn, T. P. Ma, Ferroelectric field effect transistors for memory applications. *Adv. Mater.* **22**, 2957–2961 (2010).
7. S. Kim, H. Y. Jeong, S. K. Kim, S.-Y. Choi, K. J. Lee, Flexible memristive memory array on plastic substrates. *Nano Lett.* **11**, 5438–5442 (2011).
8. C.-B. Eom, S. Trolier-McKinstry, Thin-film piezoelectric MEMS. *MRS Bull.* **37**, 1007–1021 (2012).
9. W. S. Wong, A. Salleo, Eds., *Flexible Electronics: Materials and Applications* (Springer, 2009).
10. S. R. Forrest, The path to ubiquitous and low-cost organic electronic appliances on plastic. *Nature* **428**, 911–918 (2004).
11. N. Izyumskaya, Y.-I. Alivov, S.-J. Cho, H. Morkoç, H. Lee, Y.-S. Kang, Processing, structure, properties, and applications of PZT thin films. *Crit. Rev. Solid State Mater. Sci.* **32**, 111–202 (2007).
12. M. T. Ghoneim, M. A. Zidan, M. Y. Alnassar, A. N. Hanna, J. Kosel, K. N. Salama, M. M. Hussain, Thin PZT-based ferroelectric capacitors on flexible silicon for nonvolatile memory applications. *Adv. Electron. Mater.* **1**, 1500045–1500054 (2015).
13. M. T. Ghoneim, M. M. Hussain, Study of harsh environment operation of flexible ferroelectric memory integrated with PZT and silicon fabric. *Appl. Phys. Lett.* **107**, 052904–052908 (2015).
14. Z. Zuo, B. Chen, Q.-f. Zhan, Y. Liu, H. Yang, Z. Li, G. Xu, R.-W. Li, Preparation and ferroelectric properties of freestanding $Pb(Zr,Ti)O_3$ thin membranes. *J. Phys. D Appl. Phys.* **45**, 185302–185306 (2012).
15. A. I. Kingon, S. Srinivasan, Lead zirconate titanate thin films directly on copper electrodes for ferroelectric, dielectric and piezoelectric applications. *Nat. Mater.* **4**, 233–237 (2005).
16. C. T. Shelton, B. J. Gibbons, Epitaxial $Pb(Zr,Ti)O_3$ thin films on flexible substrates. *J. Am. Ceram. Soc.* **94**, 3223–3226 (2011).
17. J. Rho, S. J. Kim, W. Heo, N. E. Lee, H. S. Lee, J.-H. Ahn, $PbZr_xTi_{1-x}O_3$ Ferroelectric thin-film capacitors for flexible nonvolatile memory applications. *IEEE Electron Device Lett.* **31**, 1017–1019 (2010).
18. I. Bretos, R. Jiménez, A. Wu, A. I. Kingon, P. M. Vilarinho, M. L. Calzada, Activated solutions enabling low-temperature processing of functional ferroelectric oxides for flexible electronics. *Adv. Mater.* **26**, 1405–1409 (2014).
19. W. Y. Kim, H. C. Lee, Stable ferroelectric poly (vinylidene fluoride-trifluoroethylene) film for flexible nonvolatile memory application. *IEEE Electron Device Lett.* **33**, 260–262 (2012).
20. D. Mao, M. A. Quevedo-Lopez, H. Stiegler, B. E. Gnade, H. N. Alshareef, Optimization of poly(vinylidene fluoride-trifluoroethylene) films as non-volatile memory for flexible electronics. *Org. Electron.* **11**, 925–932 (2010).
21. G.-G. Lee, E. Tokumitsu, S.-M. Yoon, Y. Fujisaki, J.-W. Yoon, H. Ishiwara, The flexible non-volatile memory devices using oxide semiconductors and ferroelectric polymer poly(vinylidene fluoride-trifluoroethylene). *Appl. Phys. Lett.* **99**, 012901–012903 (2011).
22. R. H. Kim, H. J. Kim, I. Bae, S. K. Hwang, D. B. Velusamy, S. M. Cho, K. Takaishi, T. Muto, D. Hashizume, M. Uchiyama, P. André, F. Mathevet, B. Heinrich, T. Aoyama, D.-E. Kim, H. Lee, J.-C. Ribierre, C. Park, Non-volatile organic memory with sub-millimeter bending radius. *Nat. Commun.* **5**, 3583–3594 (2014).
23. J. Liu, Z. Yin, X. Cao, F. Zhao, L. Wang, W. Huang, H. Zhang, Fabrication of flexible, all-reduced graphene oxide non-volatile memory devices. *Adv. Mater.* **25**, 233–238 (2013).
24. Y. Ji, B. Cho, S. Song, T.-W. Kim, M. Choe, Y. H. Kahng, T. Lee, Stable switching characteristics of organic nonvolatile memory on a bent flexible substrate. *Adv. Mater.* **22**, 3071–3075 (2010).
25. M. Owczarek, K. A. Hujsak, D. P. Ferris, A. Prokofjevs, I. Majerz, P. Szklarz, H. C. Zhang, A. A. Sarjeant, C. L. Stern, R. Jakubas, S. Hong, V. P. Dravid, J. F. Stoddart, Flexible ferroelectric organic crystals. *Nat. Commun.* **7**, 13108–13117 (2016).
26. S. R. Bakaul, C. R. Serrao, M. Lee, C. W. Yeung, A. Sarker, S. L. Hsu, A. K. Yadav, L. Dedon, L. You, A. I. Khan, J. D. Clarkson, C. Hu, R. Ramesh, S. Salahuddin, Single crystal functional oxides on silicon. *Nat. Commun.* **7**, 10547–10551 (2016).
27. A. Koma, Van der Waals epitaxy for highly lattice-mismatched systems. *J. Cryst. Growth* **201–202**, 236–241 (1999).
28. W. Jaegermann, A. Klein, C. Pettenkofer, *Electron Spectroscopies Applied to Low-Dimensional Materials* (Springer, 2002), pp. 317–402.
29. C.-I. Li, J.-C. Lin, H.-J. Liu, M.-W. Chu, H.-W. Chen, C.-H. Ma, C.-Y. Tsai, H.-W. Huang, H.-J. Lin, H.-L. Liu, P.-W. Chiu, Y.-H. Chu, Van der Waal epitaxy of flexible and transparent VO_2 film on muscovite. *Chem. Mater.* **28**, 3914–3919 (2016).
30. C.-H. Ma, J.-C. Lin, H.-J. Liu, T. H. Do, Y.-M. Zhu, T. D. Ha, Q. Zhan, J.-Y. Juang, Q. He, E. Arenholz, P.-W. Chiu, Y.-H. Chu, Van der Waals epitaxy of functional MoO_2 film on mica for flexible electronics. *Appl. Phys. Lett.* **108**, 253104–253108 (2016).
31. Y. Bitla, C. Chen, H.-C. Lee, T. H. Do, C.-H. Ma, L. V. Qui, C.-W. Huang, W.-W. Wu, L. Chang, P.-W. Chiu, Y.-H. Chu, Oxide heteroepitaxy for flexible optoelectronics. *ACS Appl. Mater. Interfaces* **8**, 32401–32407 (2016).
32. P.-C. Wu, P.-F. Chen, T. H. Do, Y.-H. Hsieh, C.-H. Ma, T. D. Ha, K.-H. Wu, Y.-J. Wang, H.-B. Li, Y.-C. Chen, J.-Y. Juang, P. Yu, L. M. Eng, C.-F. Chang, P.-W. Chiu, L. H. Tjeng, Y.-H. Chu, Heteroepitaxy of Fe_3O_4/muscovite: A new perspective for flexible spintronics. *ACS Appl. Mater. Interfaces* **8**, 33794–33801 (2016).
33. C. B. Eom, R. B. Van Dover, J. M. Phillips, D. J. Werder, J. H. Marshall, C. H. Chen, R. J. Cava, R. M. Fleming, D. K. Fork, Fabrication and properties of epitaxial ferroelectric heterostructures with ($SrRuO_3$) isotropic metallic oxide electrodes. *Appl. Phys. Lett.* **63**, 2570–2572 (1993).
34. C. Simbrunner, G. Hernandez-Sosa, M. Oehzelt, T. Djuric, I. Salzmann, M. Brinkmann, G. Schwabegger, I. Watzinger, H. Sitter, R. Resel, Epitaxial growth of sexithiophene on mica surfaces. *Phys. Rev. B* **83**, 115443–115450 (2011).

Downloaded from http://advances.sciencemag.org/ on June 11, 2017

35. E. Strelcov, Y. Kim, J. C. Yang, Y. H. Chu, P. Yu, X. Lu, S. Jesse, S. V. Kalinin, Role of measurement voltage on hysteresis loop shape in piezoresponse force microscopy. *Appl. Phys. Lett.* **101**, 192902–192905 (2012).
36. K.-I. Park, J. H. Son, G.-T. Hwang, C. K. Jeong, J. Ryu, M. Koo, I. Choi, S. H. Lee, M. Byun, Z. L. Wang, K. J. Lee, Highly-efficient, flexible piezoelectric PZT thin film nanogenerator on plastic substrates. *Adv. Mater.* **26**, 2514–2520 (2014).
37. H.-J. Tseng, W.-C. Tian, W.-J. Wu, Flexible PZT thin film tactile sensor for biomedical monitoring. *Sensors* **13**, 5478–5492 (2013).
38. C. Dagdeviren, B. D. Yang, Y. Su, P. L. Tran, P. Joe, E. Anderson, J. Xia, V. Doraiswamy, B. Dehdashti, X. Feng, B. Lu, R. Poston, Z. Khalpey, R. Ghaffari, Y. Huang, M. J. Slepian, J. A. Rogers, Conformal piezoelectric energy harvesting and storage from motions of the heart, lung, and diaphragm. *Proc. Natl. Acad. Sci. U.S.A.* **111**, 1927–1932 (2014).
39. E. D. Tsagarakis, C. Lew, M. O. Thompson, E. P. Giannelis, Nanocrystalline barium titanate films on flexible plastic substrates via pulsed laser annealing. *Appl. Phys. Lett.* **89**, 202910–202912 (2006).
40. K. Saiki, K. Ueno, T. Shimada, A. Koma, Application of Van der Waals epitaxy to highly heterogeneous systems. *J. Cryst. Growth* **95**, 603–606 (1989).
41. K. Ueno, K. Saiki, T. Shimada, A. Koma, Epitaxial growth of transition metal dichalcogenides on cleaved faces of mica. *J. Vac. Sci. Technol. A* **8**, 68–72 (1990).
42. Z. Suo, E. Y. Ma, H. Gleskova, S. Wagner, Mechanics of rollable and foldable film-on-foil electronics. *Appl. Phys. Lett.* **74**, 1177–1179 (1999).
43. Y. He, H. Dong, Q. Meng, W. Shao, L. He, W. Hu, Mica, a potential two-dimensional-crystal gate insulator for organic field-effect transistors. *Adv. Mater.* **46**, 5502–5507 (2011).

Acknowledgments: We acknowledge A. Q. Jiang and Z.-L. Bai, Fudan University, for their help in PUND measurements. **Funding:** This work was supported by the Ministry of Science and Technology, Republic of China (MOST 103-2119-M-009-003-MY3 and MOST 104-2628-E-009-005-MY2), and National Natural Science Foundation of China (grant no. 11032010). **Author contributions:** J.J., Y.B., Y.-C.Z., and Y.-H.C. conceived and designed the experiments. J.J. carried out the sample preparation and ferroelectric measurements. Y.-H.H. did the scanning probe microscopy measurement. H.-J.L. performed the XRD measurement. C.-H.M. and P.-W.C. performed RHEED measurements. C.-W.H., T.H.D., Y.-H.L., and W.-W.W. contributed to the TEM experiment. J.J., Y.B., C.-W.H., T.H.D., H.-J.L., Y.-H.H., and Y.-H.C. analyzed the data. C.-Y.J. and Y.-C.C. performed the Raman measurements. Y.B. and Y.-H.C. co-wrote the paper with contributions from all the authors. **Competing interests:** The authors declare that they have no competing interests. **Data and materials availability:** All data needed to evaluate the conclusions in the paper are present in the paper and/or the Supplementary Materials. Additional data related to this paper may be requested from the authors.

Submitted 11 January 2017
Accepted 14 April 2017
Published 9 June 2017
10.1126/sciadv.1700121

Citation: J. Jiang, Y. Bitla, C.-W. Huang, T. H. Do, H.-J. Liu, Y.-H. Hsieh, C.-H. Ma, C.-Y. Jang, Y.-H. Lai, P.-W. Chiu, W.-W. Wu, Y.-C. Chen, Y.-C. Zhou, Y.-H. Chu, Flexible ferroelectric element based on van der Waals heteroepitaxy. *Sci. Adv.* **3**, e1700121 (2017).

Downloaded from http://advances.sciencemag.org/ on June 11, 2017

Flexible ferroelectric element based on van der Waals heteroepitaxy
Jie Jiang, Yugandhar Bitla, Chun-Wei Huang, Thi Hien Do, Heng-Jui Liu, Ying-Hui Hsieh, Chun-Hao Ma, Chi-Yuan Jang, Yu-Hong Lai, Po-Wen Chiu, Wen-Wei Wu, Yi-Chun Chen, Yi-Chun Zhou and Ying-Hao Chu (June 9, 2017)
Sci Adv 2017, 3:.
doi: 10.1126/sciadv.1700121

This article is publisher under a Creative Commons license. The specific license under which this article is published is noted on the first page.

For articles published under CC BY licenses, you may freely distribute, adapt, or reuse the article, including for commercial purposes, provided you give proper attribution.

For articles published under CC BY-NC licenses, you may distribute, adapt, or reuse the article for non-commerical purposes. Commercial use requires prior permission from the American Association for the Advancement of Science (AAAS). You may request permission by clicking here.

The following resources related to this article are available online at http://advances.sciencemag.org. (This information is current as of June 11, 2017):

Updated information and services, including high-resolution figures, can be found in the online version of this article at:
http://advances.sciencemag.org/content/3/6/e1700121.full

Supporting Online Material can be found at:
http://advances.sciencemag.org/content/suppl/2017/06/05/3.6.e1700121.DC1

This article **cites 38 articles,** 1 of which you can access for free at:
http://advances.sciencemag.org/content/3/6/e1700121#BIBL

Downloaded from http://advances.sciencemag.org/ on June 11, 2017

Science Advances (ISSN 2375-2548) publishes new articles weekly. The journal is published by the American Association for the Advancement of Science (AAAS), 1200 New York Avenue NW, Washington, DC 20005. Copyright is held by the Authors unless stated otherwise. AAAS is the exclusive licensee. The title Science Advances is a registered trademark of AAAS